Measurement of guided mode wavenumbers in soft tissue–bone mimicking phantoms using ultrasonic axial transmission

2012 Phys. Med. Biol. 57 3025

(http://iopscience.iop.org/0031-9155/57/10/3025)

IOP Publishing Physics in Medicine and Biology

Phys. Med. Biol. **57** (2012) 3025–3037 doi:10.1088/0031-9155/57/10/3025

Measurement of guided mode wavenumbers in soft tissue–bone mimicking phantoms using ultrasonic axial transmission

Jiangang Chen[1], Josquin Foiret[2,3], Jean-Gabriel Minonzio[2,3], Maryline Talmant[2,3], Zhongqing Su[1], Li Cheng[1] and Pascal Laugier[2,3]

[1] Department of Mechanical Engineering, The Hong Kong Polytechnic University, Kowloon, Hong Kong
[2] UPMC (Univ Paris 6) Laboratoire d'Imagerie Paramétrique F-75005, Paris, France
[3] CNRS, UMR 7623, LIP, 15 rue de l'école de médecine F-75006, Paris, France

E-mail: jean-gabriel.minonzio@upmc.fr

Received 30 August 2011, in final form 29 February 2012
Published 26 April 2012
Online at stacks.iop.org/PMB/57/3025

Abstract

Human soft tissue is an important factor that influences the assessment of human long bones using quantitative ultrasound techniques. To investigate such influence, a series of soft tissue–bone phantoms (a bone-mimicking plate coated with a layer of water, glycerol or silicon rubber) were ultrasonically investigated using a probe with multi-emitter and multi-receiver arrays in an axial transmission configuration. A singular value decomposition signal processing technique was applied to extract the frequency-dependent wavenumbers of several guided modes. The results indicate that the presence of a soft tissue-mimicking layer introduces additional guided modes predicted by a fluid waveguide model. The modes propagating in the bone-mimicking plate covered by the soft-tissue phantom are only slightly modified compared to their counterparts in the free bone-mimicking plate, and they are still predicted by an elastic transverse isotropic two-dimensional waveguide. Altogether these observations suggest that the soft tissue–bone phantoms can be modeled as two independent waveguides. Even in the presence of the overlying soft tissue-mimicking layer, the modes propagating in the bone-mimicking plate can still be extracted and identified. These results suggest that our approach can be applied for the purpose of the characterization of the material and structural properties of cortical bone.

(Some figures may appear in colour only in the online journal)

1. Introduction

The axial transmission technique, employing a set of emitter(s) and receiver(s) to measure long bones, like tibia and radius, is considered to be one of the most promising modalities among quantitative ultrasound (QUS) techniques. The shaft of long bones has been evidenced to act as a natural waveguide (Moilanen 2008, Talmant *et al* 2010). A number of studies have demonstrated experimentally the potential of this technique to assess bone mechanical and structural properties (Moilanen *et al* 2003a, Bossy *et al* 2004, Muller *et al* 2005). Several *in vivo* studies evidenced that the velocity of the first-arrival signal (FAS) allows discriminating osteoporotic from healthy patients (Moilanen *et al* 2003a, Knapp *et al* 2001, Barkmann *et al* 2000, Hans *et al* 1999, Talmant *et al* 2009, Kilappa *et al* 2011). In other studies, the signal processing techniques were adapted to identify several guided modes propagating in long bones, focusing on their velocity dispersion or attenuation properties. For example, the energetic late arrival (ELA), associated with the low frequency fundamental flexural A_0-like plate guided mode, has been measured *in vitro* in human radius specimens (Moilanen *et al* 2006, Sasso *et al* 2009). Higher order guided modes have also been observed *in vitro* in bovine and human bone specimens (Lefebvre *et al* 2002, Lee and Yoon 2004, Le *et al* 2010, Protopappas *et al* 2006, Song *et al* 2011, Tatarinov *et al* 2011). In the above-mentioned reports, the experiments were conducted *in vitro* on excised bones specimens, i.e., after removal of the overlying soft tissue.

While the feasibility of the identification and measurement of multiple guided modes has been demonstrated on long bones without overlying soft tissue on top of it, the influence of soft tissue on guided modes dispersion curves has not been extensively studied yet, apart from the studies reported by Moilanen *et al* (2008) dedicated to the fundamental flexural mode, i.e., A_0 in a plate or F_{11} in a tube. Previous *in vivo* studies by these authors suggested that the measurement of a signal contribution consistent with the fundamental flexural mode was possible *in vivo* on the tibia in some patients (Moilanen *et al* 2003a, Moilanen *et al* 2007), while in other patients the identification of such a mode was difficult, presumably due to the presence of soft tissues on top of the bone. In a subsequent modeling study (Moilanen *et al* 2008), the authors reported an increasing mode density when the soft tissue thickness increases. From that latter study, the authors concluded that the identification of the flexural mode might be difficult when the soft tissue on top of the bone is thicker than a few millimeters. The presence of the soft tissue layer on top of long bones may be the cause for the ambiguity encountered in mode identification *in vivo* for some patients.

Our group has recently introduced a method for extracting guided mode phase velocities based on the singular value decomposition (SVD). This method consist in the analysis of the time responses for all possible pairs of emitter-receiver of a multi-emitter and multi-receiver array placed on top of the bone being investigated (Minonzio *et al* 2010, 2011a). High order guided modes are obtained from the maxima of the so-called *Norm* function in the temporal frequency—spatial frequency plane. The method has been shown to be efficient on bone-mimicking plates made of a dissipative transverse isotropic elastic medium with characteristics mimicking those of actual bones (Minonzio *et al* 2011b).

The goal of this work was to investigate the effect of overlying soft tissues on the propagation characteristics of guided modes in an axial transmission configuration by extending the method to the determination of the guided modes dispersion curves for a fluid–solid bilayer waveguide consisting of soft tissue-mimicking fluid or viscoelastic layers on top of a bone-mimicking plate. Our assumption is that the bilayer waveguide behaves as two uncoupled waveguides. Since the bone-mimicking plate is a transverse isotropic solid and soft tissue-mimicking fluid is isotropic media, the problem in this study is described using a

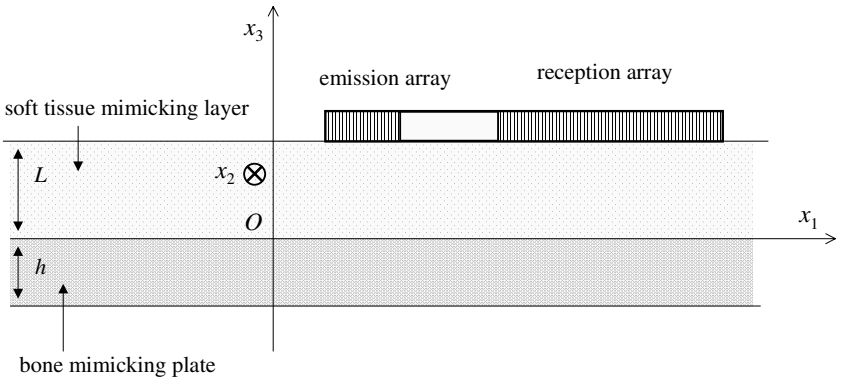

Figure 1. Geometry of the problem: an elastic plate, covered by a fluid layer, is inspected with a multi-emitter and multi-receiver array.

two-dimensional model. The theory of guided mode propagation in plates is briefly summarized in section 2, where the dispersion equations for a fluid plate and for a transverse isotropic elastic plate are reminded. The experimental procedure using a multi-element transmitting and receiving transducer array is described in section 3, where we outline some specifics of the SVD-based signal processing technique. In section 4, the results of axial transmission experiments on a variety of bilayer waveguides designed to mimic the overlying soft tissues on top of cortical bone are displayed. The measured guided mode wavenumbers are compared to the theoretical predictions for the two uncoupled fluid and solid waveguides model. We conclude by a discussion of our results and a summary of our findings.

2. Theoretical model

In an axial transmission measurement configuration, a linear array of emitters and receivers is aligned along the bone axis (Ox_1 in figure 1). In spite of the tubular shape of long bones, the propagation of guided waves in the cortical layer can be described in a first approximation by a plate model (Moilanen 2008, Talmant *et al* 2010). The plate model will thus be considered hereinafter. Consider a solid plate of thickness h covered by a fluid layer of thickness L (figure 1). The wavenumbers of the bilayer guided modes can be theoretically computed (Dayal and Kinra 1989, Yapura and Kinra 1995, Simonetti 2004). They depend on the thicknesses, the mass densities, the plate elastic coefficients C_{ij} and the fluid longitudinal velocity c_f. However, for simplicity, following Simonetti (2004) and Wu and Yang (2011), the bilayer waveguide is assumed in a first approximation to behave mainly like two decoupled waveguides. It implies that a measured guided mode wavenumber $k^{\exp}$ corresponds to either a plate k^p or a fluid wavenumber k^f. This approximation will be discussed in section 4.

First, consider a fluid layer of thickness L with clamped-free boundary conditions (figure 1). The boundary conditions implies that the wavenumber k_3 along the (Ox_3) direction is equal to $(n+1/2)\pi/L$, with n an integer. Moreover, the wavenumber k_1 along the (Ox_1) direction satisfies $k_1^2 + k_3^2 = (\omega/c_f)^2$, with ω the angular frequency and c_f the longitudinal velocity in fluid. Thus the fluid-guided wavenumber, denoted k^f and equal to k_1 satisfies (Royer and Dieulesaint 2000, Simonetti 2004)

$$k^f = \left[\left(\frac{\omega}{c_f}\right)^2 - \left(\frac{[n+1/2]\,\pi}{L}\right)^2\right]^{1/2}, \tag{1}$$

The different fluid guided modes are labeled according to their index n equal to 0, 1, 2, 3, ...

Secondly, consider a free transverse isotropic elastic plate of thickness h (figure 1). The direction (Ox_1) is the symmetry axis. Guided waves in the elastic plate are different from their counterparts in the fluid layer as the elastic plate supports the propagation of shear waves. Because the probe works in piston mode and does not excite horizontal shear displacement, only motion in the plane (Ox_1x_3) is considered. Thus a two-dimensional approximation can be considered (Dayal and Kinra 1989, Rhee *et al* 2007). Following previous conditions, the relation between k_3 and k_1 satisfies (Dayal and Kinra 1989, Rhee *et al* 2007)

$$k_{3\pm}^2 = \left(\frac{-M \pm \sqrt{M^2 - 4N}}{2} \right)^2 k_1^2, \tag{2}$$

where the sign $\pm$ indicates the positive and negative (Ox_3) directions (figure 1). The terms M and N correspond to

$$M = \frac{C_{11}C_{33} - C_{33}C_{55} - C_{13}^2 - \frac{\rho\omega^2}{k_1^2}(C_{33} + C_{55})}{C_{33}C_{55}}, \tag{3a}$$

$$N = \frac{\left(\frac{\rho\omega^2}{k_1^2} - C_{11}\right)\left(\frac{\rho\omega^2}{k_1^2} - C_{55}\right)}{C_{33}C_{55}}, \tag{3b}$$

where ρ is the plate density, ω is the angular frequency, and C_{11}, C_{33}, C_{13} and C_{55} are the stiffness coefficients of the transverse isotropic plate. Following equation (32) of Rhee *et al* (2007), the dispersion equation of the symmetric Lamb modes S_n can be written as

$$\begin{aligned}(C_{33}R_-k_{3-} + C_{13}k_1)(R_+k_1 + k_{3+})\sin(k_{3+}h)\cos(k_{3-}h) \\ -(C_{33}R_+k_{3+} + C_{13}k_1)(R_-k_1 + k_{3-})\sin(k_{3-}h)\cos(k_{3+}h) = 0.\end{aligned} \tag{4a}$$

Following equation (34) of Rhee *et al* (2007), the dispersion equation for the anti-symmetric modes A_n is obtained by inverting the + and – subscripts inside the parentheses in (4*a*)

$$\begin{aligned}(C_{33}R_+k_{3+} + C_{13}k_1)(R_-k_1 + k_{3-})\sin(k_{3+}h)\cos(k_{3-}h) \\ -(C_{33}R_-k_{3-} + C_{13}k_1)(R_+k_1 + k_{3+})\sin(k_{3-}h)\cos(k_{3+}h) = 0.\end{aligned} \tag{4b}$$

The terms R_+ and R_- in (4) are given by

$$R_\pm = \frac{\left(\rho\omega^2 - C_{11}k_1^2 - C_{55}k_{3\pm}^2\right)}{(C_{55} + C_{13})k_1k_{3\pm}}. \tag{5}$$

In the following, the theoretical wavenumbers k_f, associated with guided modes in the soft tissue-mimicking layer, will be computed using (1). Likewise, the theoretical wavenumbers k^p, associated with the bone-mimicking plate, will be computed using (2) to (5), with k^p equal to k_1. These theoretical wavenumbers will be compared with experimental data $k^{\exp}$ in section 4 measured on a bone-mimicking plate covered by various soft tissue-mimicking layers. The experimental data are obtained using the experimental set-up and the signal processing described in section 3.

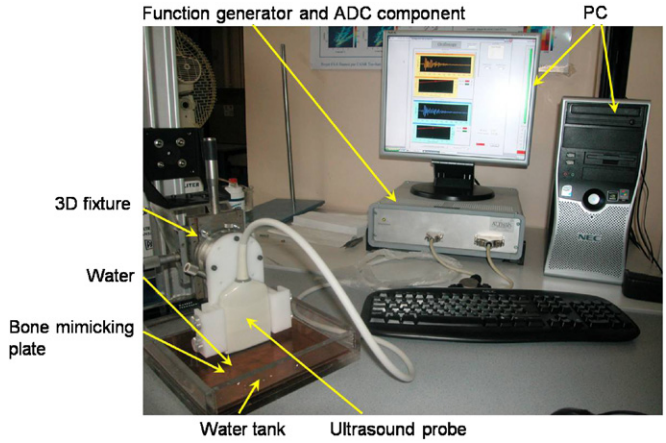

Figure 2. Experimental set-up.

Table 1. Elastic coefficients of the bone-mimicking plate.

Elastic coefficients	C_{11}	C_{33}	C_{55}	C_{13}
Numerical values (GPa)	22.5	13.5	4.1	5.9

3. Material and method

3.1. Experimental set-up

In order to acquire experimental data to compare with the model described in section 2, a custom made linear transducer array (Vermon, Tours, France) was used (figures 1 and 2). The characteristics of this probe have already been given in previous papers by our group (Minonzio *et al* 2010, 2011a). The probe contains $N^{\mathrm{E}} = 5$ emitters and $N^{\mathrm{R}} = 32$ receivers (pitch of the array: 0.8 mm; minimum distance between both transmitting and receiving arrays: 11 mm; central frequency 1 MHz; −6 dB spectrum spanning the frequency range of 0.5 to 1.5 MHz and the −20 dB spectrum spanning the frequency range of 0.4 to 1.8 MHz). Such a configuration allowed 160 transmission-reception channels. During the measurement, each emitter was excited with wideband pulses. The radiofrequency signals recorded on the receivers were digitized (8 bits, 20 MHz, 1024 time samples) and finally stored on a computer for off-line analysis. Twenty radiofrequency signals were time averaged to increase signal-to-noise ratio. The driving electronics has been manufactured by Althaïs Technology (Tours, France).

A 2.3 mm thick bone-mimicking plate (Sawbones®, Pacific Research Laboratories, Washington, USA) was used as a bone phantom. The thickness is typical of the cortical thickness of the human radius. The plate is made of oriented glass fibers embedded in epoxy. Its elastic properties, summarized in table 1, are close to those of actual bones. The mass density ρ of the bone-mimicking plate is equal to 1.64 g.cm^{-3}. The stiffness coefficients C_{11}, C_{33}, C_{44} and C_{55} were deduced from bulk compression and shear velocities measured using contact transducers (Minonzio *et al* 2011b, Granke *et al* 2011). The stiffness coefficient C_{13} was deduced from C_{33} and C_{44} using $C_{13} = C_{33} - 2C_{44}$.

Table 2. Longitudinal velocity c_f, density ρ and attenuation α of the different soft tissue-mimicking materials considered in the experiments.

Material	c_f (ms^{-1})	ρ (gcm^{-1})	α (dB.cm^{-1}) at 1 MHz	References
Silicon rubber	1230	0.8	1	(Itsumi *et al* 2009, Zheng *et al* 2011)
Water	1480	1.0	10^{-2}	(Tang *et al* 1988, Culjat *et al* 2010)
Soft tissues	1430–1600	0.95–1.05	0.5–1	(Culjat *et al* 2010, Mast 2000)
Glycerol (98%)	1910	1.26	0.2	(Bossy *et al* 2004, Fergusson *et al* 1954, Tang *et al* 1988, Figueiredo *et al* 2009)

Three different soft tissue-mimicking layers have been used: water, 98% glycerol (VWR International, Fontenay-sous-Bois, France) and silicon rubber. The silicon rubber was artificially produced by mixing three substances, i.e. 4600A, 4600B and AK35 (all from Wacker Chemicals Ltd, Béziers, France) with the proportions of 1:0.1:1.6. The longitudinal velocity c_f, density ρ and attenuation α of the three soft-tissue phantoms are given in table 2. The longitudinal velocity in the silicon has been measured using two contact transducers. These materials, easy to handle, were chosen, owing to the similarity of their acoustical properties with those of soft tissues (table 2). Water is similar to soft tissues in term of velocity. Silicon rubber, 98% glycerol and soft tissue have similar attenuation values. The longitudinal velocities in the silicon rubber and 98% glycerol are respectively lower and higher than that in soft tissues. These materials have been used in order to test the model with a wide range of longitudinal velocity and attenuation values. Moreover, considering that soft tissues are not pure fluid but sustains shear stresses (Moilanen *et al* 2003b), silicon rubber is used as a tissue equivalent material (Njeh *et al* 1999).

The bone phantom was placed into a tank, and supported by four tiny cylinders (height: 2 mm). First, reference measurements were taken with the bone-mimicking phantom measured without any soft tissue-mimicking layer on top of it, with the probe being simply coupled to the bone plate with an acoustically transparent gel (Aquasonic®, Parker Laboratories, Inc., NJ, USA). Subsequently, the fluid (water or 98% glycerol) was introduced into the tank. The position and the parallelism of the probe with respect to the plate could be adjusted by tuning the translational and rotational stages (figure 2). The position of the probe was adjusted above the plate to leave a 4 mm thick and then 8 mm thick layer of water, and subsequently a 4 mm thick layer of 98% glycerol. Following the measurements with water and 98% glycerol, a 4 mm thick layer of silicon rubber was placed on top of the bone-mimicking plate, such that any air bubbles in between could be carefully eliminated. The gel was used to improve the coupling between the probe and the silicon rubber.

3.2. Signal processing

The SVD-based signal processing technique has been described in detail elsewhere (Minonzio *et al* 2010, 2011a). Only the main steps are recalled here. The recorded radiofrequency signals $r_{ij}(t)$, with i and j the emission and reception indices ranging from 1 to N^{E} and 1 to N^{R}, respectively, are first Fourier-transformed. The singular value decomposition is subsequently applied to the $N^{\mathrm{E}} \times N^{\mathrm{R}}$ sub-matrices, i.e. the matrices $R_{ij}(f)$ at each frequency. The signal subspace is determined by applying a first threshold t_1 on the singular values. The singular values below that threshold are considered associated with the noise subspace. The M singular values above this threshold are associated with the signal subspace and their associated reception singular vectors, denoted $\mathbf{U}_n$, are a basis of the experimental guided modes. The

threshold t_1 is heuristically selected. Then, the so-called *Norm* function is defined by the following equation:

$$\text{Norm}\,(f,k) = \sum_{n=1}^{M} |\langle \mathbf{U}_n |\ \mathbf{e}^{pw}\ (k)\rangle|^2, \tag{6}$$

where $\mathbf{e}^{pw}(k)$ corresponds to a spatial plane wave at the spatial frequency k defined on the reception array. Its norm is defined equal to 1.

The scalar product $\langle \mathbf{U}_0 | \mathbf{e}^{pw}(k)\rangle$ corresponds to the normalized spatial Fourier transform of the singular vector $\mathbf{U}_n$. Thus, the SVD can be interpreted as a denoising step between the temporal and spatial Fourier transforms. If k corresponds to a guided mode wavenumber k_{exp}, the *Norm* function is close to 1, and the guided mode is projected in the singular vectors basis. If k does not correspond to a guided mode wavenumber, the *Norm* function is small compared to 1. Subsequently, a second heuristically chosen threshold t_2 is applied to the *Norm* function, the values of which larger than this threshold correspond to the guided modes wavenumbers k_{exp}.

As an example, the case of the 2.3 mm thick bone-mimicking plate alone (i.e. without fluid layer on top) is discussed. First, the corresponding *Norm* function given by (6) is shown in figure 3(a) in the (f, k) plane. The retained maxima correspond to the experimental wavenumbers k^{exp} are marked with crosses in figure 3(b). They are compared with the theoretical plate modes k^p computed from (2) to (5), using the stiffness coefficients given in table 1. The modes are labeled S_n or A_n according to their symmetry or anti-symmetry nature and their cutoff frequency × thickness product (denoted $f_c.h$). Three modes with transverse asymptotic behavior are identified: A_1 ($f_c.h = c_T{}^{\perp}/2$), S_2 ($c_T{}^{\perp}$), S_4 ($2c_T{}^{\perp}$), where c_T denotes the shear wave velocity, and the superscript $^{\perp}$ the direction perpendicular to the fibers (Minonzio *et al* 2011b). Moreover, one mode (S_1) with longitudinal asymptotic behavior is identified ($f_c.h = c_L{}^{\perp}/2$), with $c_L{}^{\perp}$ being the compression wave velocity in the direction perpendicular to the fibers. The S_0 mode is also measured at low frequencies. The experimentally derived guided modes wavenumbers $k_{\text{exp}}(f)$ are overall in good agreement with the theoretical Lamb modes wavenumbers.

4. Experimental results and discussion

With the afore-addressed model and method, the coupling effect of soft tissue was interrogated by introducing four different soft tissue-mimicking layers over the bone-mimicking plate: water (layer thickness: 4 and 8 mm), 98% glycerol (layer thickness: 4 mm) and silicon rubber (layer thickness: 4 mm). The results obtained with the four soft tissue-mimicking layers on top of the bone-mimicking bone plate are shown in figure 4. The experimental wavenumbers k^{exp} are plotted against frequency together with the theoretical guided modes wavenumbers of the free bone-mimicking plate k^p (already presented in figure 3) and of the fluid layers. The wavenumbers of the theoretical guided modes in the free fluid layers, denoted k^f, are computed using (1) and the fluid velocity values given in table 2. The fluid modes are labeled with integers, denoted n, starting from 0.

A visual examination of the results shown in panels a and b of figure 4 reveals that the fluid–solid bilayer supports the propagation of additional modes compared to the bone-mimicking plate alone (figure 3). There is an overall agreement between these new modes and the theoretical predictions from the fluid layer model, even in the case of viscoelastic soft tissue-mimicking media (98% glycerol or silicon). Note also that the modes of the silicon

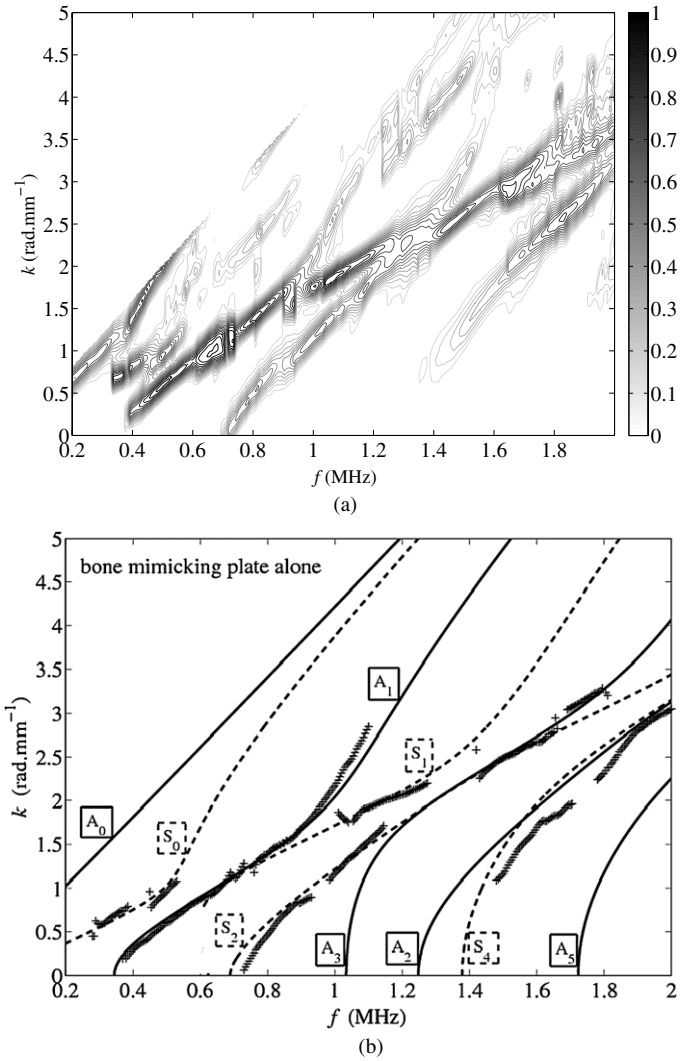

Figure 3. *Norm* function from the 2.3 mm thick bone-mimicking plate alone (a) and corresponding experimental guided mode wavenumbers $k^{\exp}$ (black crosses), obtained from the *Norm* function maxima, compared with theoretical plate modes k^p, shown with black continuous (anti-symmetric A_n) and dashed (symmetric S_n) lines (b).

layer, which behaves more like a soft viscoelastic solid than a fluid, are still predicted by the fluid model. In addition, such an agreement is evaluated using

$$\text{error} = \sqrt{\frac{\sum_f \left\| k_n^{\exp} - k_n^{\text{th}} \right\|^2}{\sum_f \left\| k_n^{\exp} \right\|^2}}, \tag{7}$$

where k_nth corresponds to nth theoretical fluid (k_f) or plate (k_p) mode. For the plate modes, the errors are equivalent with (figure 4) or without (figure 3) the fluid layer. The error ranges

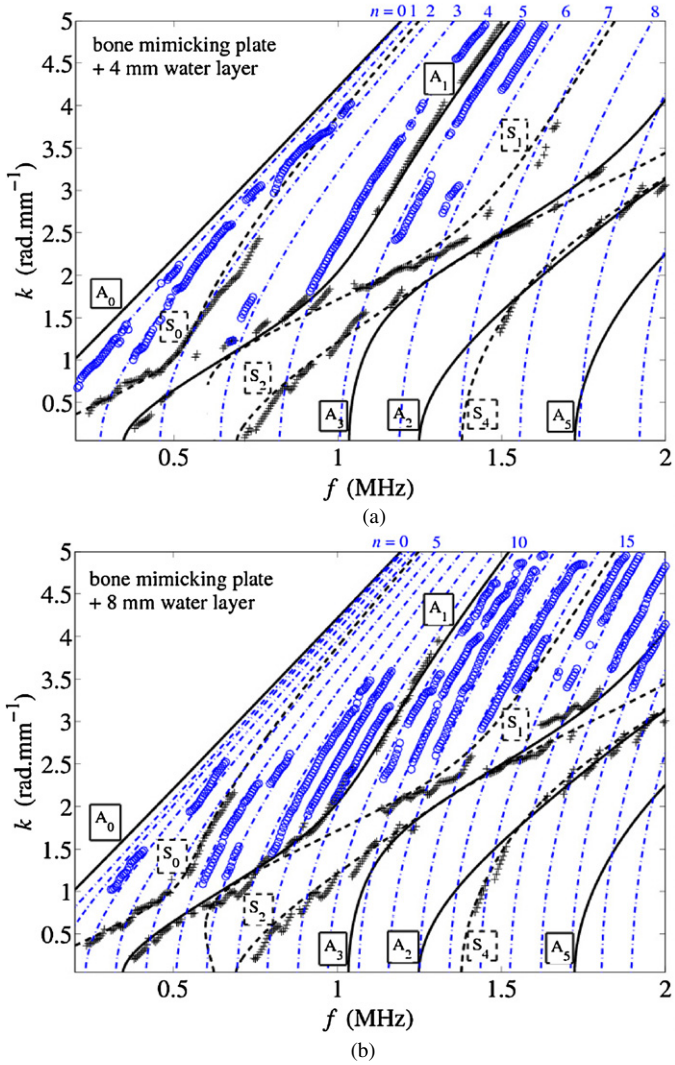

Figure 4. Experimental guided mode wavenumbers k^{exp} (blue circles and black crosses) obtained from the bone-mimicking plate in the presence of a soft tissue-mimicking layer: 4 mm thick water layer (a); 8 mm thick water layer (b); 4 mm thick 98% glycerol layer (c); 4 mm thick silicon rubber (d). The experimental wavenumbers are compared with the theoretical plate Lamb modes k^p, shown with black continuous (anti-symmetric A_n) and dashed (symmetric S_n) lines and theoretical fluid layer modes k^f, shown with blue dashed-dot lines (labeled with index n). The experimental wavenumbers are shown with symbols: black crosses are associated with plate modes, blue circles are associated with fluid layer modes.

from 4% (A_1 and S_1) to 9% (S_0, S_2 and S_4). For the fluid modes, the error varies from 2% ($n =$ 4 in the 4 mm water case) to 20% ($n = 7$ in the 4 mm glycerol case). The average of the fluid mode error for the four cases is equal to 5%.

The number of observed fluid-guided waves increases with the layer thickness L as predicted by the model. For instance, more modes are observed for the 8 mm thick water layer (panel b), with n ranging from 3 to 17, than for the 4 mm thick water layer (panel a), with n

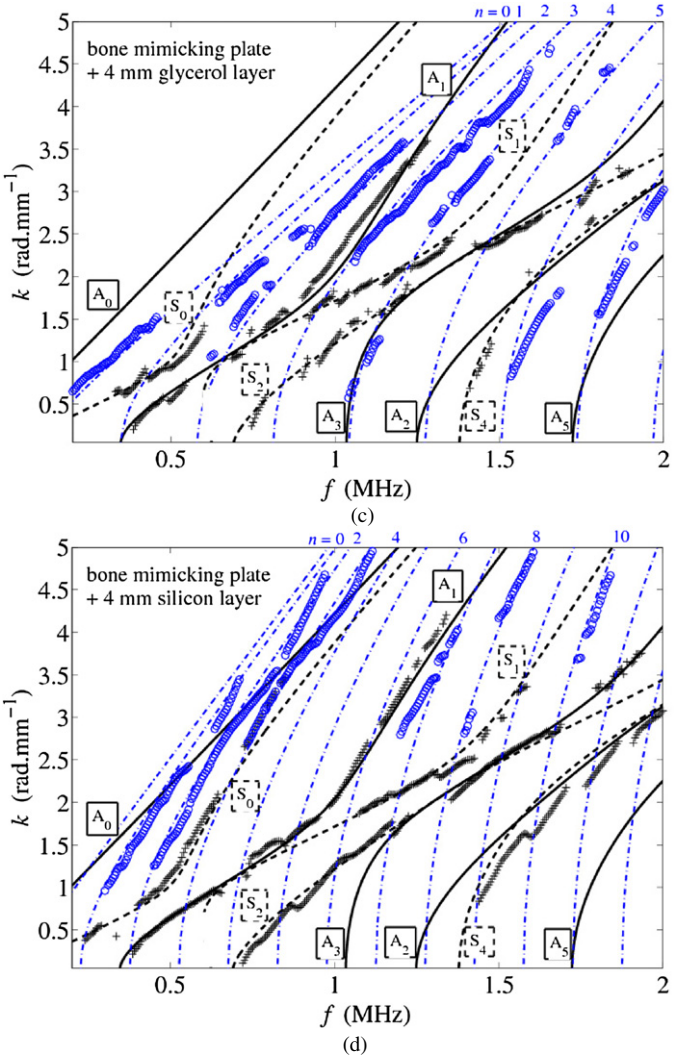

Figure 4. (Continued.)

ranging from 0 to 6. The slopes of the dispersion curves of the fluid guided modes tend toward ω/c_f as the frequency increases (equation (1)). Thus considering the 4 mm thick fluid layers only, the slope of the dispersion curves at high frequencies are steeper for the silicon (panel d), compared to water (panel a) and 98% glycerol (panel c) in agreement with the values given in table 2.

These additional modes are marked with circles on figure 4, whereas the experimental wavenumbers associated with the bone-mimicking plate modes are marked with crosses. The criteria for resolving the question of whether an observed trace is the result of a mode propagating in the soft tissue-mimicking layer or in the bone-mimicking plate are the distances between the experimental trace and the simulated traces: an experimental trace is associated to the closest theoretical dispersion curve. In the present study, mode selection remains purely manual. For most of the cases, both the fluid and bone-mimicking plate modes do not overlap

so that their differentiation is trivial. When two modes overlap, the proper mode identification remains ambiguous, as is the case for mode S_0 which overlaps with the water layer mode $n = 2$ (panel a) and $n = 4$ (panel b) or for the mode A_3 which overlaps with the 98% glycerol layer mode $n = 4$ (panel c).

While most of the modes associated with the bone-mimicking plate with the soft tissue-mimicking layer on top of it (figure 4, panels a–d) remain almost unchanged compared to their counterparts observed on the free bone-mimicking plate (figure 3), and are still predicted by an elastic transverse isotropic waveguide, we note slight differences like discontinuities in the trace of mode A_1 (panels a and c) or scalloping in the traces of mode S_1 and S_2 (panel b), presumably due to interferences with the fluid guided modes. However, these differences remain small, and should not prevent mode identification for the purpose of bone characterization.

We proposed to model the fluid–solid bilayer assemblies that were specifically designed to mimic the soft tissue layer on top of long bones as two uncoupled fluid and solid waveguides, each of which supporting its own guided modes. Results from theoretical computations based on this hypothesis appear to be consistent with measurements of both fluid and solid guided modes depending upon specific details of the soft tissue-mimicking layer considered.

These observations suggest that the modes propagating in the bone-mimicking plate can be extracted and identified in presence of the soft tissue-mimicking layer. Toward this goal, one needs to properly model the frequency-dependent wavenumbers of the soft tissue layer, which should be feasible once the thickness of the soft tissue has been estimated, from simple pulse echo measurements for example. Note that the speed of sound in the soft tissue is also required for the model. But because the speed of sound in soft biological tissues is fairly constant, its value derived from the literature should be sufficient. It is then conceivable that meaningful bone properties can be recovered by carrying out an inversion scheme comparing the identified cortical bone modes to a theoretical plate model.

There are limitations to the preliminary work described in this brief report. The main limitation, of course, is that the measurements are performed in phantoms instead of actual bones. The phantoms only approximate the structure and acoustical properties of soft tissue and cortical bone. Additional complexities will arise from the inhomogeneity of real soft tissues and bones. It is not clear yet whether *in vivo* application of this approach will be feasible, until a range of experimental data has been analyzed. An advantage of the present study is that a custom made probe designed for clinical examinations (Talmant *et al* 2009) has been used to conduct experiments on the phantoms. On the other hand, a plate model has been used in the study, while long bones are tubular-shaped. However, previous studies of axial transmission in cortical bone have previously demonstrated a high level of consistency of the plate model with experimental data (Moilanen *et al* 2006).

5. Conclusion

In summary, this study of the coupling effect of soft tissue-mimicking layers on top of a bone-mimicking plate on guided wave propagation suggests that the presence of a soft tissue-mimicking layer introduces additional guided modes, but that both layers can be considered as independent waveguides. These results indicate that the modes propagating in the bone-mimicking plate can still be identified using an elastic transverse isotropic two-dimensional waveguide model and that they could be used for the purpose of the characterization of the material and structural properties of the bone waveguide. Future studies will be extended to *in vivo* measurements.

Acknowledgments

This work has been supported by ANR project 'COSTUM' 09-TECS-005-03 (2009–2012).

References

Barkmann R, Kantorovich E, Singal C, Hans D, Genant H K, Heller M and Gluer C C 2000 A new method for quantitative ultrasound measurements at multiple skeletal sites. First results of precision and fracture discrimination *J. Clin. Densitom.* **3** 1–7

Bossy E, Talmant M, Defontaine M, Patat F and Laugier P 2004 Bidirectional axial transmission can improve accuracy and precision of ultrasonic velocity measurement in cortical bone: a validation on test materials *IEEE Trans. Ultrason. Ferroelectr. Freq. Control* **51** 71–9

Culjat M O, Goldenberg D, Tewari P and Singh R S 2010 A review of tissue substitutes for ultrasound imaging *Ultrasound Med. Biol.* **36** 861–73

Dayal V and Kinra V K 1989 Leaky Lamb waves in an anisotropic plate: 1. An exact solution and experiments *J. Acoust. Soc. Am* **85** 2268–76

Fergusson F A A, Guptill E W and MacDonald A D 1954 Velocity of sound in glycerol *J. Acoust. Soc. Am.* **26** 67–9

Figueiredo M K K, Costa-Felix R P B, Alvarenga A V, Maggi L E, Portilho M F, Souza M N and Romeiro G A 2009 Study, development, and implementation of analysis technique of biphasic attenuation systems using ultrasound *Xix Imeko World Congress: Fundamental and Applied Metrology, Proceedings* (Budapest: Imeko) pp 2634–7

Granke M, Grimal Q, Saïed A, Nauleau P, Peyrin F and Laugier P 2011 Change in porosity is the major determinant of the variation of cortical bone elasticity at the millimeter scale in aged women *Bone* **49** 1020–6

Hans D, Srivastav S K, Singal C, Barkmann R, Njeh C F, Kantorovich E, Gluer C C and Genant H K 1999 Does combining the results from multiple bone sites measured by a new quantitative ultrasound device improve discrimination of hip fracture? *J. Bone Miner. Res.* **14** 644–51

Itsumi K, Hosono Y, Yamamoto N and Yamashita Y J 2009 Low acoustic attenuation silicone rubber lens for medical ultrasonic array probe *IEEE Trans. Ultrason. Ferroelectr. Freq. Control* **56** 870–4

Kilappa V, Moilanen P, Xu L, Nicholson P H F, Timonen J and Cheng S 2011 Low-frequency axial ultrasound velocity correlates with bone mineral density and cortical thickness in the radius and tibia in pre- and postmenopausal women *Osteoporos. Int.* **22** 1103–13

Knapp K M, Blake G M, Spector T D and Fogelman I 2001 Multisite quantitative ultrasound: Precision, age- and menopause-related changes, fracture discrimination, and T-score equivalence with dual-energy x-ray absorptiometry *Osteoporos. Int.* **12** 456–64

Le L H, Gu Y J, Li Y P and Zhang C 2010 Probing long bones with ultrasonic body waves *Appl. Phys. Lett.* **96** 114102

Lee K I and Yoon S W 2004 Feasibility of bone assessment with leaky Lamb waves, in bone phantoms and a bovine tibia *J. Acoust. Soc. Am.* **115** 3210–7

Lefebvre F, Deblock Y, Campistron P, Ahite D and Fabre J J 2002 Development of a new ultrasonic technique for bone and biomaterials *in vitro* characterization *J. Biomed. Mater. Res.* **63** 441–6

Mast T D 2000 Empirical relationships between acoustic parameters in human soft tissues *Acoust. Res. Lett. Online* **1** 37–42

Minonzio J G, Foiret J, Talmant M and Laugier P 2011b Impact of attenuation on guided mode wavenumber measurement in axial transmission on bone mimicking plates *J. Acoust. Soc. Am.* **130** 3574–82

Minonzio J G, Talmant M and Laugier P 2010 Guided wave phase velocity measurement using multi-emitter and multi-receiver arrays in the axial transmission configuration *J. Acoust. Soc. Am* **127** 2913–9

Minonzio J G, Talmant M and Laugier P 2011a Measurement of guided mode wave vectors by analysis of the transfer matrix obtained with multi-emitters and multi-receivers in contact *J. Phys.: Conf. Ser.* **269** 012003

Moilanen P 2008 Ultrasonic guided waves in bone *IEEE Trans. Ultrason. Ferroelectr. Freq. Control* **55** 1277–86

Moilanen P, Nicholson P H F, Kärkkäinen T, Wang Q, Timonen J and Cheng S 2003a Assessment of the tibia using ultrasonic guided waves in pubertal girls *Osteoporos. Int.* **14** 1020–7

Moilanen P, Nicholson P H F, Kilappa V, Cheng S and Timonen J 2006 Measuring guided waves in long bones: modeling and experiments in free and immersed plates *Ultrasound. Med. Biol.* **32** 709–19

Moilanen P, Nicholson P H F, Kilappa V, Wang Q, Timone J and Cheng S 2003b The role of soft tissue in ultrasonic guided wave measurement in bone *5th World Congress on Ultrasonics (WCU) (Paris, France)* pp 899–902

Moilanen P, Talmant M, Bousson V, Nicholson P H F, Cheng S, Timonen J and Laugier P 2007 Ultrasonically determined thickness of long cortical bones: two-dimensional simulations of *in vitro* experiments *J. Acoust. Soc. Am.* **122** 1818–26

Moilanen P, Talmant M, Kilappa V, Nicholson P, Cheng S L, Timonen J and Laugier P 2008 Modeling the impact of soft tissue on axial transmission measurements of ultrasonic guided waves in human radius *J. Acoust. Soc. Am.* **124** 2364–73

Muller M, Moilanen P, Bossy E, Nicholson P, Kilappa V, Timonen J, Talmant M, Cheng S and Laugier P 2005 Comparison of three ultrasonic axial transmission methods for bone assessment *Ultrasound Med. Biol.* **31** 633–42

Njeh C F, Kearton J R, Hans D and Boivin C M 1999 The use of quantitative ultrasound to monitor fracture healing: a feasibility study using phantoms *Med. Eng. Phys.* **20** 781–6

Protopappas V C, Fotiadis D I and Malizos K N 2006 Guided ultrasound wave propagation in intact and healing long bones *Ultrasound. Med. Biol.* **32** 693–708

Rhee S H, Lee J K and Lee J J 2007 The group velocity variation of Lamb wave in fiber reinforced composite plate *Ultrasonics* **47** 55–63

Royer D and Dieulesaint E 2000 *Elastic Waves in Solids I* (New York: Springer)

Sasso M, Talmant M, Haiat G, Naili S and Laugier P 2009 Analysis of the most energetic late arrival in axially transmitted signals in cortical bone *IEEE Trans. Ultrason. Ferroelectr. Freq. Control* **56** 2463–70

Simonetti F 2004 Lamb wave propagation in elastic plates coated with viscoelastic materials *J. Acoust. Soc. Am.* **115** 2041–53

Song X, Ta D and Wang W 2011 Analysis of superimposed ultrasonic guided waves in long bones by the joint approximative diagonalization of eigen-matrices algorithm *Ultrasound Med. Biol.* **37** 1704–13

Talmant M, Foiret J and Minonzio J G 2010 *Bone Quantitative Ultrasound Chap. 7 Guided Waves in Cortical Bones* (New York: Springer) pp 147–79

Talmant M, Kolta S, Roux C, Haguenauer D, Vedel I, Cassou B, Bossy E and Laugier P 2009 *In vivo* performance evaluation of bi-directional ultrasonic axial transmission for cortical bone assessment *Ultrasound Med. Biol.* **35** 912–9

Tang X, Toksöz M, Tarif P and Wilkens R 1988 A method for measuring acoustic wave attenuation in the laboratory *J. Acoust. Soc. Am.* **83** 453–62

Tatarinov A, Sarvazyan A, Beller G and Felsenberg D 2011 Comparative examination of human proximal tibiae *in vitro* by ultrasonic guided waves and pQCT *Ultrasound Med. Biol.* **37** 1791–801

Yapura C L and Kinra V K 1995 Guided-waves in a fluid solid bilayer *Wave Motion* **21** 35–46

Wu C H and Yang C H 2011 Guided waves propagating in a bi-layer system consisting of a piezoelectric plate and a dielectric fluid layer *IEEE Trans. Ultrason. Ferroelectr. Freq. Control* **58** 1612–8

Zheng Y P, Chen J and Ling H Y 2011 Development of an ultrasound platform for the evaluation of plantar soft tissue properties: a feasibility study on silicone phantom feet *Instrum. Sci. Technol.* **39** 248–60